SENSITIVITY OF PURGE FLOW EFFECTS TO DIFFERENT HIGH WORK TURBINE DESIGNS

K. Regina, Reza S. Abhari

Laboratory for Energy Conversion
Department of Mechanical and Process
Engineering, ETH Zurich
Zurich, Switzerland

Anestis I. Kalfas

Department of Mechanical Engineering
Aristotle University of Thessaloniki
Thessaloniki, Greece

Abstract

An experimental study of hub purge flow from the rotor upstream rim seal gap on the performance of a highly loaded turbine stage with two different aerodynamic designs is presented in this paper. The test configuration consists of a one-and-a-half stage, unshrouded, highly loaded axial turbine with two different sets of blading, which are representative of low aspect ratio high work gas turbines.

Efficiency measurements performed with a pneumatic probe at the exit of the rotor for several purge flow injection levels show a reduction of efficiency of 0.8 % per percent of injected purge mass flow for both aerodynamic designs. However, the different designs yield a different spanwise extent where the hub injection has a detrimental impact on the efficiency.

Time-resolved measurements at rotor inlet and rotor exit performed with the in-house developed Fast Response Aerodynamic Probe (FRAP) reveal the sources for the different behavior of the stage designs: The unsteady interaction of the purge flow with the secondary flows of the main flow and the dominant impact on the pulsating radial displacement of the rotor hub passage vortex show a magnitude which is sensitive to the stage design. The maximum penetration depth of the core of the rotor hub passage vortex shows a difference of 10 % - 15 % span for the different designs, leading to an increased level of interaction between the secondary flows from the hub and the casing for the stage design with the higher penetration depth of the rotor hub passage vortex.

Vorticity measurements are used for correlating the strength of the rotor hub passage vortex and its intensification by the injected amount of purge flow with the unsteady penetration depth of the rotor hub passage vortex. The two stage designs yield a different sensitivity of the vorticity and circulation of the rotor hub passage vortex indicating the sensitivity of the purge flow related periodic variation of penetration depth to the stage design.

Nomenclature

Variables:

$\overline{c}_{abs}$	mean absolute flow velocity	[m/s]
c_{ax}	axial flow velocity	[m/s]
c_p	specific heat capacity	[J/kg/K]

i	incidence angle	[°]
IR	injection rate	[%]
$\dot{m}$	mass flow	[kg/s]
M	torque	[Nm]
N	rotational speed	[rpm]
p	pressure	[Pa]
R	hub radius	[m]
T	temperature	[K]
U	local rotational speed	[m/s]
γ	isentropic coefficient	[-]
η	isentropic efficiency	[-]
μ	dynamic viscosity	[Pa s]
Π	pressure ratio	[-]
ρ	density	[kg/m^3]
φ	flow yaw angle	[°]
Φ	flow coefficient	[-]
ψ	loading coefficient	[-]
ω	angular frequency	[1/s]

Subscripts:

0	stagnation flow quantity
in	turbine inlet flow quantity
rel	relative frame flow quantity
tt	total-to-total

Abbreviations:

FOR	frame of reference
FRAP	Fast Response Aerodynamic Probe
HPV	hub passage vortex
IP	intermediate pressure
LP	low pressure
NGV	nozzle guide vane
RMS	root mean square

Introduction

In modern gas turbines, the ingestion of hot gases from the main flow into the disk cavities between the rotors and the stators is prevented by bypassing cooling purge flow from the compressor and injecting it through the stator/rotor rim seal. This ensures a safe operation of the machines by avoiding the ingress of hot gases into these cavities, minimizing the risk of local overheating. However, this seal mechanism is used for mechanical integrity reasons and has a strong adverse impact on the aerodynamics of the turbine potentially reducing the turbine efficiency.

The injection of purge flow results in highly complex mixing processes and interaction mechanisms with the secondary flows of the main annulus and it has a strongly 3-dimensional and unsteady character, which is difficult to numerically predict by means of commonly used computational methods.

In order to keep the computational expenses in a reasonable frame and find a practicable compromise between computational costs and accuracy, modern turbines are often designed with CFD methods, which do not detail these complex interaction mechanisms and processes.

It is well reported in open literature that there are several different factors during the operation of a gas turbine which set the minimum amount of purge mass flow to make the seal mechanism effective. Worth mentioning are a temperature fluctuation criterion given by Kobayashi et al. [1], a pressure criterion used by Chew et al. [2], a factor depending on the seal geometry and the rotational Reynolds number given by Dadkah et al. [3]. However, e.g. Gentilhomme et al. [4] report on deviations between an ingestion model and measurements of seal effectiveness for high injection rates and based on numerical simulations, Jakoby et al. [5] report on large scale unsteady features in wheelspaces for a specific range of sealant mass flow.

Also the impact of the purge flow injection on the main flow of HP turbines is reported in literature. McLean et al. [6] found the changes in efficiency to be strongly dependent on the type of injection configuration. Paniagua et al. [7] related the increased penetration depth of the rotor HPV

coming along with increasing purge mass flows to the lower temperature of the purge flow. Ong et al. [8] attributed the intensification of the rotor HPV and the increase in penetration depth to the negative incidence resulting from the purge flow. The periodic nature of the penetration depth of the rotor HPV has been shown by Ong et al. [8], Schuepbach et al. [9] and Regina et al. [10].

The present work addresses and quantifies experimentally the impact of the injection of purge flow on the isentropic total-to-total efficiency of two low aspect HP turbines with different aerodynamic designs under the same operating conditions. For improving understanding of the purge flow interaction mechanisms in a HP turbine, the impact of the purge flow on both stage designs is compared. Since both turbine stages have not been especially designed for the unsteady interaction mechanisms associated to the purge flow, the current work aims to evaluate the robustness of the stage designs towards the changes in the flow field caused by the injection of the purge flow.

Experimental Method

The experimental study was carried out in the research axial turbine facility "LISA" in the Laboratory for Energy Conversion at ETH Zurich. The one-and-a-half stage unshrouded turbine is representative for a high work, cooled turbine.

Research Turbine Facility
The research turbine facility consists of a quasi-closed air loop which includes a single stage radial compressor, a two stage water-to-air heat exchanger and a calibrated venturi nozzle for high accuracy mass flow measurements. In order to ensure a homogeneous flow field, there is a 3-m-long flow conditioning stretch upstream of the turbine test section. Additionally, the flow undergoes an acceleration

ahead of the turbine to reduce the significance of any remaining flow non-uniformities from upstream. Downstream of the turbine test section, the air loop is open to atmospheric conditions. A DC generator absorbs the power of the turbine and controls the rotational speed with an indicated accuracy of ±0.02 % (±0.5 rpm). Figure 1 shows a schematic of the test rig and its main components.
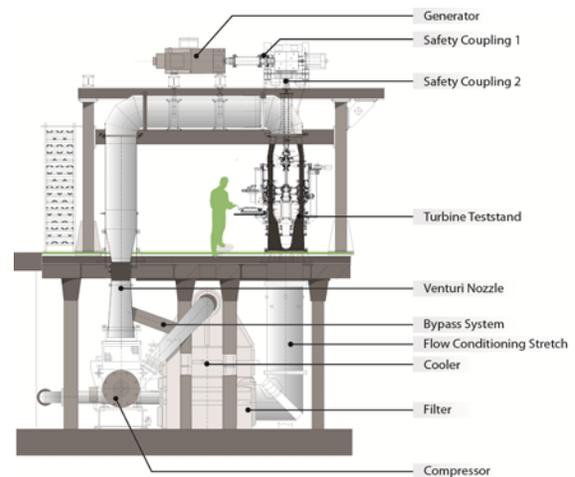
Figure 1: Schematic of the test rig "LISA" at ETH Zurich

The inlet total temperature $T_{0,in}$ is controlled by the water-to-air heat exchanger to an accuracy of ±0.3 K. A torquemeter is used for the measurement of the torque on the rotor shaft. As the compressor pressure ratio is limited to $\Pi_{c,max}$ = 1.5, it is necessary to add a tandem deswirl vane arrangement to recover the static pressure at the exit of the second stator back to the ambient level in order to reach the intended turbine pressure ratio of $\Pi_{t,1.5}$ = 1.65. The unshrouded rotor has a nominal tip clearance gap of 1 % of the span and the variation of the tip clearance gap between different assemblies is less than 1 % of the gap ensuring good repeatability. At the exit of the first stator, the flow is compressible with an average Mach number of 0.53.

The current turbine configurations are derived from the design

presented by Behr et al. [11]. The most salient differences are an increased blade row spacing between the first stator and the rotor, an increased axial clearance at the exit of the hub cavity, where the purge flow is injected ("Design A"), as well as additionally a modified profile stacking in the first stator and a more aft-loaded rotor with reduced leading edge radius ("Design B").

Operating conditions

During the measurements of both turbine design configurations, the 1.5 stage total-to-static pressure ratio is kept constant at $\Pi_{t,1.5} =$ 1.65 in order to account for the change in ambient pressure on different days. With the same purpose, the pressures are non-dimensionalized by the respective inlet stagnation pressure. The main operating parameters are summarized in Table 1.

Table 1: Operating conditions and geometrical characteristics

Pressure ratio $\Pi_{t,1.5}$ $[-]$	1.650 ± 0.006
Inlet total temperature $T_{0,in}$ $[K]$	327.9 ± 0.3
Capacity $\frac{\dot{m}\sqrt{T_{0,in}}}{p_{0,in}}$ $\left[\frac{kg \cdot K^{1/2}}{s \cdot bar}\right]$	151.8 ± 0.2
Non-dimensional speed $\frac{N}{\sqrt{T_{0,in}}}$ $\left[\frac{rps}{K^{1/2}}\right]$	2.49 ± 0.05
Mach nr $[-]$ (S1,ex/R,ex/S2,ex)	0.53/0.26/0.48
Reynolds nr $[\times 10^5]$ (S1 / R / S2)	7.1/3.8/5.1
Blade count $[-]$ (S1 / R / S2)	36/54/36
Aspect ratio $[-]$ (S1 / R / S2)	0.87/1.17/0.82

The purge flow injected from the rotor upstream stator/rotor cavity is an off-take from the primary air loop upstream of the flow conditioning stretch and is measured by means of a standard nozzle. The bypassed air passes a plenum and is fed through ten different nozzle guide vanes into the cavity underneath the stator platform, labeled as B in Figure 2, where a schematic of the purge flow path is depicted.
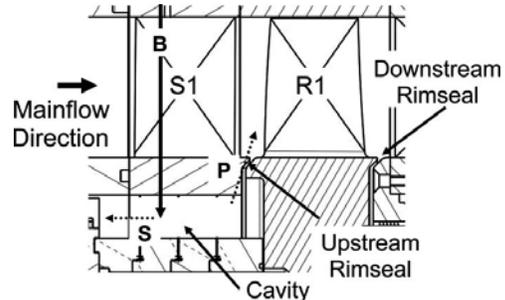
Figure 2: Schematics of the purge flow path [15] (Dimensions distorted)

After the purge flow enters the under platform cavity, there are two paths, which are indicated by dotted arrows in Figure 2. One path is through the upstream rim seal into the main flow, labeled as P. The rest of the gas, called secondary mass flow and labeled as S in Figure 2, is ejected through the drum into the atmosphere, after being measured in an additional standard nozzle. Since the pressure difference across the downstream rim seal is controlled to be zero, the net mass flow through the downstream rim seal can be assumed to be zero. As a consequence, the mass flow P eventually injected into the main flow can be calculated as the difference between the measured bypass mass flow B and the measured secondary mass flow S.

In the present investigation, the injection levels were set using the definition of the injection rate (IR) given by Equation 1.

$$IR = \frac{\dot{m}_B - \dot{m}_S}{\dot{m}_{MAIN}} \cdot 100 \qquad (1)$$

The current tests have been conducted with IR1A=-0.1% for the

design A (representing a moderate sucking from the main flow) and IR1B=0.4% for design B, as well as for IR2=0.8% and IR3=1.2% for both designs respectively. These injection rates are considered to be representative for real engine conditions.

Measurement Technology

The steady flow field at the exit of the rotor is measured with a miniature cobra-head five-hole probe (5 HP) with a tip diameter as small as 0.9 mm, whereas at the inlet to the rotor a pneumatic miniature four-hole probe (4 HP) with a cylindrical head and a diameter of 1.8 mm is used.

The unsteady flow field measurements are conducted using a Fast Response Aerodynamic Probe (FRAP), which was developed in-house at the LEC at ETH Zurich. Details on the FRAP probe and measurement technique are described in depth in Kupferschmied et al. [12] and Pfau et al. [13]. The FRAP is capable of capturing the unsteady flow features up to frequencies of 48 kHz based on measurements including the total and static pressure, flow yaw and pitch angles and Mach number. The frequency bandwidth of the temperature is limited to a frequency of 10 HZ. However, the influence of the temperature on the velocity is judged to be very modest. The FRAP has a tip diameter of 1.8 mm and is equipped with two miniature silicon piezo-resistive pressure sensors. The probe is operated in a virtual-4-sensor mode to measure the 3-dimensional, time-resolved flow properties. The data is acquired at a sampling rate of 200 kHz over a period of time of 2 s. The post processing is done for three consecutive rotor pitches. The sampling rate resolves 82 points in the rotor relative frame of reference. The typical measurement uncertainties obtained with FRAP for a calibration range of ±24° for the yaw angle and ±20° for the pitch angle are given in Table 2. The relative uncertainties and static pressures are given as a percentage of the dynamic head.

Table 2: Relative uncertainty bandwidth of the FRAP

Yaw angle	Pitch angle	P_t	P_s
0.24°	0.36°	1 %	1.2 %

The measurement data is acquired at two different axial locations in the turbine test section. By traversing the probe in radial and circumferential direction, axial plane measurements are performed. The first traverse plane, labeled with "R_{in}" is located upstream of the rotor at a distance of 16%±2% of the axial chord of the rotor. This axial location is situated above the platform leading edge of the rotor. The second traverse plane, labeled as "R_{ex}", is located downstream of the rotor at a distance of 15%±2% of the rotor axial chord. The spatial resolution of the measurement grid at these traverse planes consists of 38 points in radial and 41 points in circumferential direction covering one pitch of the first stator. The circumferential grid points are equidistant, whereas the radial points are clustered near the end walls.

Results and Discussions

In the frame of the current study, the focus of the flow field analysis is put on the rotor exit and the comparison of the sensitivities with respect to purge flow variation of both stage designs. However, also the flow field at the inlet to the rotor shall be briefly characterized for a better understanding of the origination of the complex mechanisms of purge flow.

As was mentioned by Cao et al. [14], shown by Schuepbach et al. [15] and reported by the authors in a previous publication [10], the purge flow inherent mixing processes have a clear influence on the unsteadiness of the flow field. Subsequently, the rms values of the random part of the pressure signal

acquired by means of FRAP has proven to be a good indicator for the mixing processes related to the purge flow injection and convection. The random part of the pressure signal $p'(t)$ is calculated as the difference between the time-resolved pressure signal $p(t)$ and the phase-lock averaged pressure signal $\overline{p}(t) + \tilde{p}(t)$, as given in Equation 2.

$$p(t) = \overline{p}(t) + \tilde{p}(t) + p'(t) \qquad (2)$$

More specifically, the rms of the random part of the pressure signal of the *central hole* (p_1') will be used in the following.

Rotor inlet flow field

The unsteadiness of the flow field at the inlet to the rotor as measured with FRAP show a sensitivity with respect to the injected purge flow revealing that the mixing process of the purge flow has already started at this location and it has a clear impact on the flow field. In Figure 3 the time averaged and circumferentially mass weighted rms(p_1') at the plane R_{in} are depicted for both stage designs under consideration.

The comparison of the radial distribution of the unsteadiness shows an effect due to purge flow which extends up to midspan for the design A and which is contained below 20% span for the case of the design B. These measurements prove the effectiveness of the sealing arrangement by means of an overlapping buffer arm in the cavity of the design B. Subsequently, the entrainment of the purge flow into the main flow is lower for this design. In terms of flow field unsteadiness, the incoming flow field to the rotor is influenced in a more reduced and more contained way by the purge flow injection in the case of the design B.
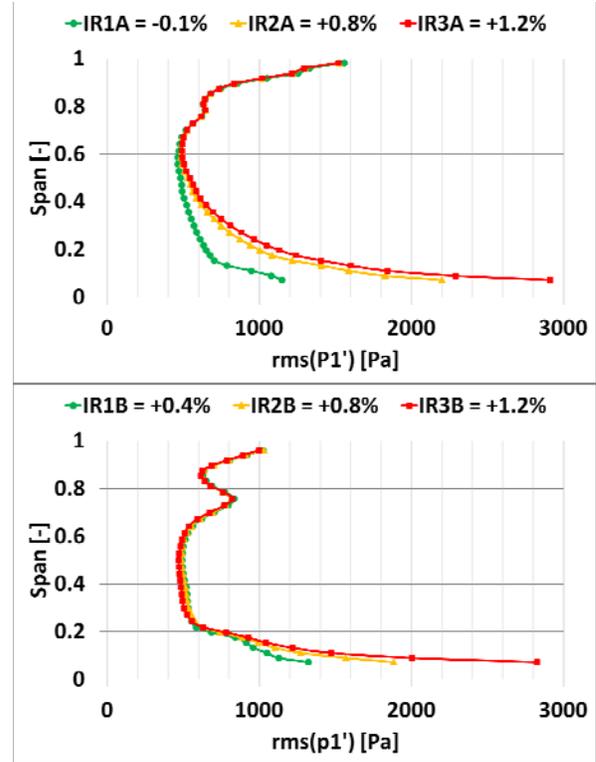
Figure 3: Time averaged and circumferentially mass weighted rms(p_1') at plane R_{in} for design A (top) and design B (bottom)

A further dominant flow quantity affected by the injection of the purge flow and partly responsible for the later impact of the purge flow on the performance of the stage is the relative flow yaw angle. Due to the passive injection method, the purge flow exits from the under platform cavity without any treatment and therefore is injected as low momentum fluid, causing a negative change in relative flow yaw angle. The time averaged and circumferentially mass weighted rotor relative flow yaw angles are shown in Figure 4 for both stage designs. The comparison is focused on the lower 30% span, which is the region with the strongest differences and from where the rotor hub passage vortex will originate.
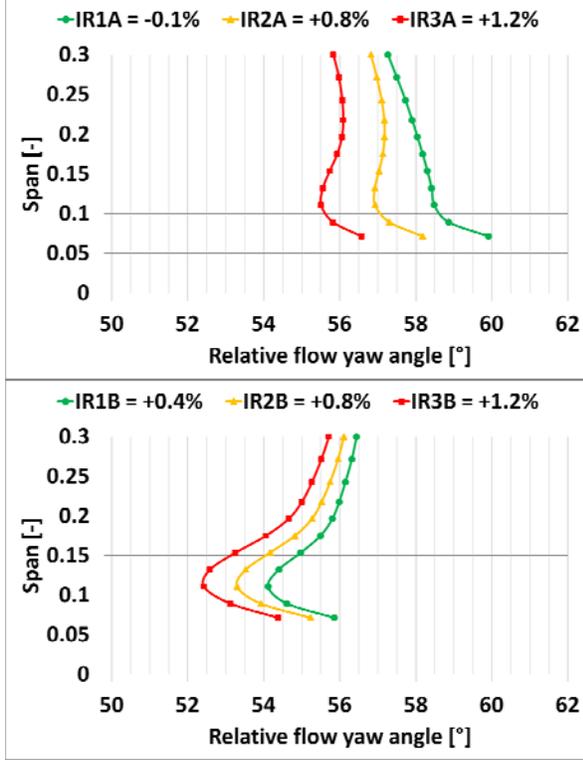
Figure 4: Time averaged and circumferentially mass weighted relative flow yaw angle at plane R_{in} for design A (top) and design B (bottom)

When comparing both sensitivities, the reduction in relative flow yaw angle due to purge flow injection is seen for both cases. However, the effect of the purge flow on the relative flow yaw angle change (incidence) is larger on the design A than on the design B. E.g at about 10% span, the incidence change amounts to -1.4° for design A and only -0.9° for design B if IR2 and IR3 are compared.

The measurement results at the rotor inlet reveal that two main drivers influencing the evolution of the purge flow mixing and convection mechanisms at the inlet to the rotor are less affected by the purge flow in the case of the design B.

Rotor exit flow field
Since both rotors have not been designed for a varying unsteady interaction of the purge flow with the main flow, the purpose of the present study is to quantify the

detrimental impact on the stage performance due to the purge flow injection and the off-design conditions introduced associated with the purge mass flow.

For this purpose, the isentropic total-to-total stage efficiency is derived from integral torque measurements and total pressure measurements with the pneumatic 5 HP at the exit of the rotor. The underlying evaluation of the efficiency is performed at every point of the measurement grid previously described and is given in Equation 3.

$$\eta_{tt} = \frac{\dfrac{\omega \cdot M}{\dot{m}_{MAIN} \cdot c_p \cdot T_{0,in}}}{1 - \left(1 - \dfrac{IR}{100}\right) \cdot \left(\dfrac{p_{0,R_{ex}}}{p_{0,in}}\right)^{(\gamma-1)/\gamma} - \dfrac{IR}{100} \cdot \left(\dfrac{p_{0,R_{ex}}}{p_{0,cav}}\right)^{(\gamma-1)/\gamma}} \tag{3}$$

Based on a linear regression, the sensitivity of the efficiency penalty due to purge flow injection amounts to $\Delta\eta_{tt}$ = -0.8% of efficiency per percent of injected purge mass flow for both stage designs tested.

However, when analyzing the performance of the rotor at different spanwise positions, the sources of efficiency penalty can be identified and differences between the two stage designs are observed. The time averaged and circumferentially mass weighted distributions of corrected total to total stage efficiency as measured for both stage designs and for the various injection rates are shown in Figure 5. For a comparison of the impact of the purge flow, the efficiencies of both stage designs have been linearly corrected to the give the value 1 at the maximum efficiency of each design.
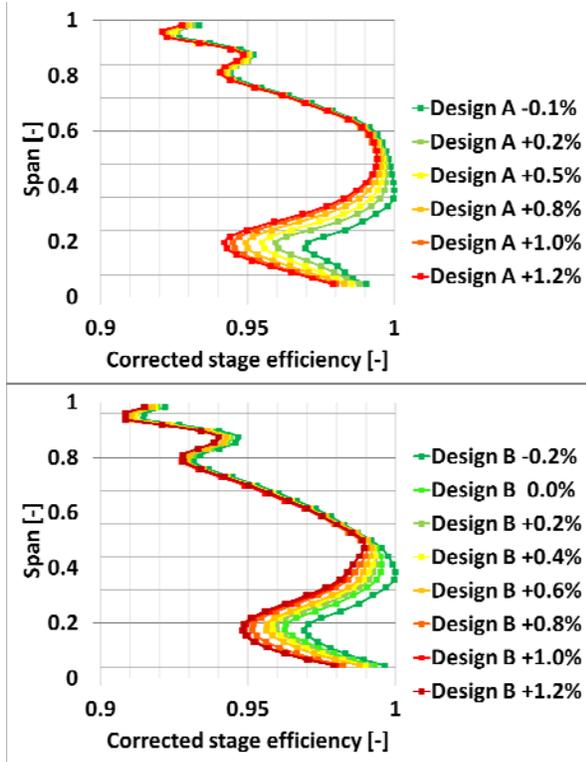
Figure 5: Time averaged and circumferentially mass weighted corrected stage efficiency at plane R_{ex} for design A (top) and design B (bottom)

The impact of the purge flow on both stage designs confirms previously reported and documented trends showing a strong impact on the stage efficiency until midspan. The present measurements confirm the dominance of the impact of the purge flow on the rotor hub passage vortex and the losses associated with it.

However, in the frame of this study, a further effect will be analyzed. The remarkable difference between the measured spanwise distributions of efficiency on the two different stage designs is the radial extent of the influence of the purge flow and the resulting impact on the performance at upper spanwise positions. E. g. at about 80% span, which is a region in the flow field predominantly affected by the tip passage vortex of the rotor, the efficiency penalty due to the purge flow injection range tested amounts to $\Delta\eta_{tt}$ = -0.2% for the design A, whereas to $\Delta\eta_{tt}$ = -0.4%

for the design B. For identifying the source of these differences, further 3D, time-resolved measurement data analysis is required.

As in the measurement plane upstream of the rotor, the unsteadiness in the flow field is characterized with the rms of the random part of the pressure signal $rms(p_1')$. After a potentially different work extraction by the rotors of the two different designs, this value is appropriate for a comparison between both design cases, since it remains unaffected by the amount of work extracted, still highlighting mixing and turbulent processes. In Figure 6, the instantaneous field contour diagrams of the $rms(p_1')$ are shown for both stage designs. The respective point in time (or relative blade-vane position) for the diagrams were chosen such to show the maximum penetration depth of the rotor hub passage vortex for each design.
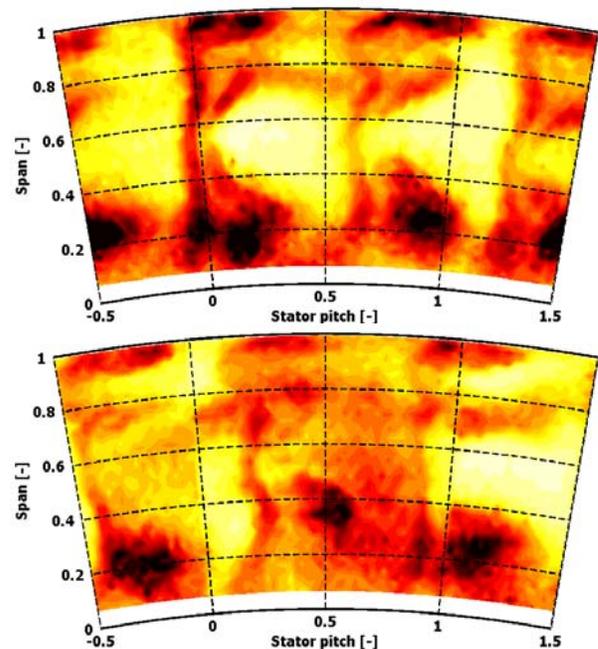
Figure 6: Instantaneous $rms(p_1')$ (non-dimensionalized) at plane R_{ex} for design A (top) and design B (bottom) for the highest IR3=+1.2%

The measurements capture and confirm the periodic nature of the penetration depth of the rotor HPV.

As shown in previous publications, the vortex core migrates towards midspan as it interacts with the purge flow injected. Since the purge flow injection upstream of the rotor occurs periodically with stator vane passing period (in the rotor frame of reference), the periodic variation of penetration depth of the rotor HPV after it convects and migrates through the rotor passage also occurs with the same periodicity.

A comparison of the time-resolved behavior as can be made with Figure 6 shows that the maximum radial location of the centre of the rotor HPV is about 25% span for the design A, while it reaches values of up to about 40% span for the design B.

It is this remarkably different migration away from the end walls, which is predominantly influenced by the injection of the purge flow, which has shown to be responsible for the influence of the casing regions by the injection of purge flow from the hub for the low aspect ratio stage design B.

In order to highlight the importance of the rotor HPV on the performance of the stage, also the streamwise vorticity shall be considered. Based on FRAP measurements at the exit plane of the rotor, the vorticity can be derived based on Equation 4.

$$\omega_S(r,\vartheta,t)=\vec{V}_{unity}\cdot\vec{\omega}=\begin{pmatrix}\overline{v}_x(r,\vartheta,t)/\overline{v}\\\overline{v}_r(r,\vartheta,t)/\overline{v}\\\overline{v}_\vartheta(r,\vartheta,t)/\overline{v}\end{pmatrix}\cdot\begin{pmatrix}\omega_x(r,\vartheta,t)\\\omega_r(r,\vartheta,t)\\\omega_\vartheta(r,\vartheta,t)\end{pmatrix} \quad (4)$$

Based on a frozen flow assumption, the radial and tangential components of the vorticity vector can be accurately approximated based on time derivatives instead of axial derivatives as was shown by Schuepbach [15].

In Figure 7, the time averaged streamwise vorticity is shown after the transformation of the data into the rotor relative frame of reference for both stage designs.
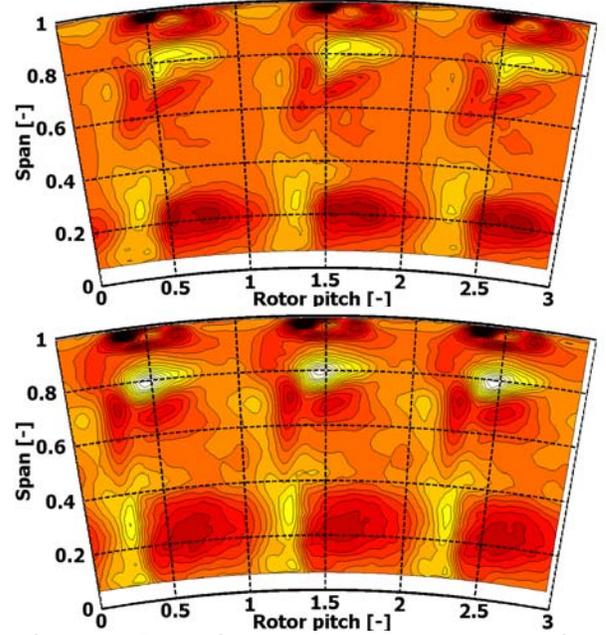
Figure 7: Time averaged streamwise vorticity (non-dimensionalized) at plane R_{ex} for design A (top) and design B (bottom) for the middle IR2=+0.8%

If both diagrams are compared, a larger zone of high positive streamwise vorticity (clockwise rotation) below 40% span associated with the rotor HPV is observed in the case of the design B. This appears together with a larger zone of high negative streamwise vorticity associated with the trailing shed vorticity, especially also at the lower 50% span. Subsequently, the design B shows a rotor exit field which is characterized by a stronger interaction zone of the vortical structures from the hub and the tip.

Due to the fact that the location of the core of the rotor hub passage vortex is varying periodically as shown in Figure 6, it is not sufficient to characterize the intensity of the vortices neither by the peak vorticity of the core nor by the area influenced with positive vorticity. For this reason, the circulation inside of the region in-

fluenced by the rotor HPV is integrated.

In a first step, the region affected by the rotor HPV is isolated by the iso-line of zero streamwise vorticity. In Figure 8, the isolated regions of the rotor HPV are shown for both designs.
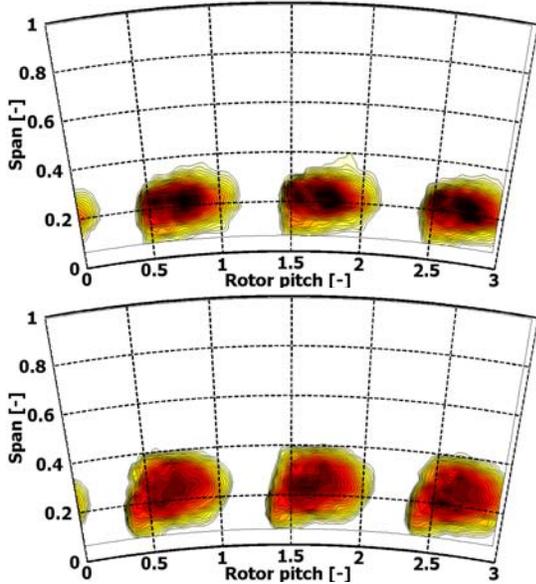
Figure 8: Time averaged streamwise vorticity (non-dimensionalized) inside of the rotor HPV at plane R_{ex} for design A (top) and design B (bottom) for the highest IR3=+1.2%

When comparing both designs based on Figure 8, the location of the core of the rotor HPV can be identified to be at about 20%-25% span based on the location of the peak vorticity in the time averaged domain. Furthermore, this location is equal for both stage designs. It becomes evident that time averaged considerations neglect the previously described present periodic location of the core of the rotor HPV, which comes along with the injection of purge flow. However, by looking only at the time averaged field, still some traces of the periodic behavior can be identified. A larger size of the area inside the iso-line of zero streamwise vorticity (by 15%) coming along with a lower peak streamwise vorticity in the centre of the area (by 12%) in

the case of the design B at the highest IR is a consequence of the periodic orbit, which is described by the core of the rotor HPV in the rotor frame of reference. Furthermore, the shape of the areas is also characteristic for the orbit and the more round shape in the design B as compared to the more oval shape of the design A, is a result of a stronger radial component of the periodic variation of penetration depth for the case of the design B.

In a second step, the areas inside of the iso-line of zero streamwise vorticity serve as the area over which the vorticity is integrated yielding the circulation. By normalization with the size of the area of integration, a mean circulation is used based on Equation 5.

$$\frac{\Psi}{A_{HPV}} = \frac{\int \varpi_s dA}{\int dA} \qquad (5)$$

Figure 9 contains the magnitude of the mean circulation of the rotor HPV for the different injection rates tested. The values were non-dimensionalized with the case of the lowest mean circulation (design A, IR1A).
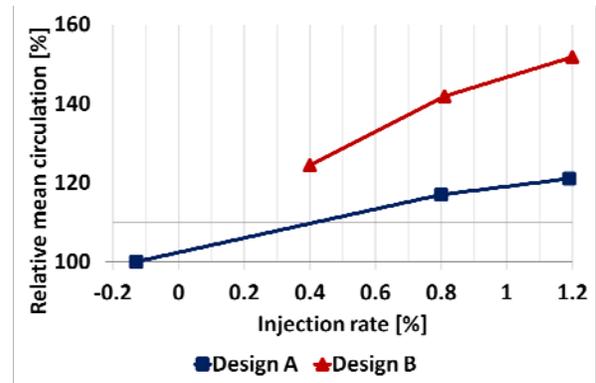
Figure 9: Mean circulation inside of rotor HPV (non-dimensionalized) at plane R_{ex} for both stage designs and all injection rates

The diagram in Figure 9 shows an overall higher level of mean circulation for the case of the design B, which is e. g. about 20% higher than

in the design A at IR2=+0.8%. Also, the higher the injection rate tested, the higher the circulation and strength of the vortex is captured. The higher strength of the rotor HPV in the design B as well as the higher sensitivity of the circulation in the design B is seen to be correlated to the larger penetration depth in the design B and to be responsible for the remarkably larger impact of the purge flow on the upper spans of the design B.

Incidence sensitivity of the rotors

Since both stage designs have not been designed for the unsteady interaction of the purge flow with the main flow, the injection of purge flow upstream of the rotor can be considered as bringing the rotor profiles to off-design conditions. For better understanding the differences between the two stage designs with respect to the off-design conditions introduced by the purge flow, the two turbines have been tested under the same overall off-design condition by reducing mass flow rate and pressure ratio of the turbine, therefore resulting in a reduced relative flow angle at the inlet to the rotor.

In Figure 10 the resulting salient impact of the off-design conditions are summarized with the time averaged and circumferentially mass weighted relative flow yaw angle at the inlet to the rotor and the stage efficiency as measured at the exit of the rotor. For both test cases, the values are given as differences of the off-design values from the nominal values at IR2 = +0.8%.
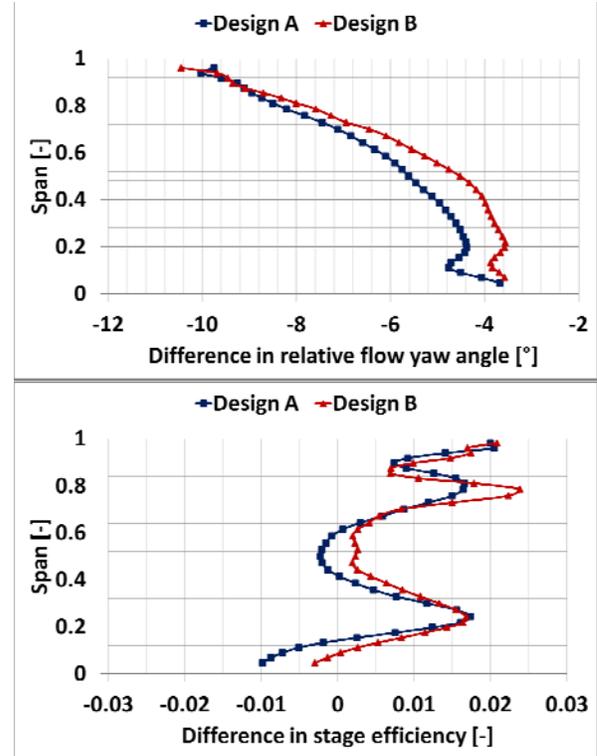
Figure 10: Time averaged and circumferentially mass weighted relative flow yaw angle difference at plane R_{in} (top) and stage efficiency difference at plane R_{ex} (bottom) for both stage designs at the middle IR2=+0.8%

The off-design measurement show a similar impact on the flow field incoming to the rotor for both designs, as the differences in relative flow yaw angle and the distribution along the span show in Figure 10. At around 20% span – in the region directly influenced by the purge flow injection at this plane – the differences are about −4°, which are in a similar range as the changes in relative flow yaw angles introduced by the purge flow (Figure 4). However, the rotor of the design A experiences a change in relative flow yaw angle, which is larger by about 1° until about midspan with respect to the changes to which design B was subject to.

Since the change in performance of the respective vanes is negligible, the changes in stage efficiency can be attributed to changes

in performance of the rotors more specifically. Although the impact on design A at the inlet to the rotor is smaller than for design B, the resulting impact on the stage efficiency is larger on design B. Integrated in radial direction, it amounts to +0.6% for the design A while to +0.9% for the design B. As a consequence, it becomes clear that for the operating conditions under consideration in the purge flow sensitivity study in the previous section, the changes in the incoming flow field have a stronger impact on the rotor of the stage design B and the rotor of the stage design A has an improved robustness with respect to changes in the incoming flow field to the rotor.

Conclusions

The results presented in this paper are based on pneumatic and aerodynamic probe measurements by means of five-hole probe and time-resolving FRAP probe, which were conducted in a one-and-a-half stage research axial turbine. The tested configuration was equipped with two sets of low aspect ratio blading representative for HP gas turbines as well as with injection of purge flow through the rotor upstream rim seal at injection rates of -0.1% (moderate sucking) and of +0.4%, +0.8% and 1.2% which are representative for real engine conditions. The most relevant differences between both stage designs are the radial stacking of the stator profiles as well as a different LE radius and the throat location of the rotor.

The measurements show a sensitivity of the purge flow effects with respect to the stage design. For stage design B, the impact of the purge flow extends to upper spanwise positions more clearly than for the other design A. In terms of the losses associated and the resulting efficiency, the design B shows an impact twice as large at these near casing spanwise positions.

By means of time-resolved FRAP measurements it is shown, that the remarkable difference of the rotor exit flow fields of both designs is a consequence of the periodic behavior of the rotor hub passage vortex, and the different penetration depth reaching values of up to 40% span in the time domain.

These observations can only be made by capturing the periodic and highly unsteady nature of the mixing process between the purge flow and the secondary flows. However:

1. Time averaged streamwise vorticity and the circulation can be taken into consideration for the characterization of the sensitivity of the impact on the rotor hub passage vortex with respect to the stage design;
2. Steady complementary measurements at off-design conditions confirm the higher robustness of one stage design with respect to changes in the incoming flow field to the rotor.

In this case, a larger leading edge radius as well as a more front-loaded rotor, as in the design A, is seen to be more beneficial for the impact of the purge flow on the evolution and the penetration depth of the rotor hub passage vortex, potentially avoiding an interaction with the secondary flow features from the casing.

Acknowledgements

References

[1] Kobayashi, N., Matsumato, M. and Shizuya, M., 1984, "An Experimental Investigation of a Gas Turbine Disk Cooling

System", Journal of Engineering for Gas Turbines and Power, Vol. 106, pp.136-141

[2] Chew, J. W., Dadkhah, S. and Turner, A. B., 1992, "Rim Sealing of Rotor-Stator Wheelspaces in the Absence of External Flow", Journal of Turbomachinery, Vol. 114, pp. 433-438

[3] Dadkhah, S., Turner, A. B. and Chew, J. W., 1992, "Performance of Radial Clearance Rim Seals in Upstream and Downstream Rotor-Stator Wheelspaces", Journal of Turbomachinery, Vol. 114, pp. 439-445

[4] Gentilhomme, O., Hills, N. J., Turner, A. B. and Chew, J. W., 2003, "Measurement and Analysis of Ingestion Through a Turbine Rim Seal", Journal of Turbomachinery, Vol. 125, pp. 505-512

[5] Jakoby, R., Zierer, T., Lindblad, K., Larsson, J., deVito, L., Bohn, D. E., Funcke, J and Decker, A., 2004, „Numerical Simulation Of The Unsteady Flow Field In An Axial Gas Turbine Rim Seal Configuration", Proceedings of ASME Turbo Expo 2004, GT2004-53829

[6] McLean, C., Camci, C. and Glezer, B., 2001, "Mainstream Aerodynamic Effects Due to Wheelspace Coolant Injection in a High-Pressure Turbine Stage: Part I – Aerodynamic Measurements in the Stationary Frame", Journal of Turbomachinery, Vol. 123, pp. 687-696

[7] Paniagua, G., Dénos, R. and Almeida, S., 2004, "Effect of the Hub Endwall cavity Flow on the Flow-Field of a Transonic High-Pressure Turbine", Journal of Turbomachinery, Vol. 126, pp. 578-586

[8] Ong, J. H. P., Miller, R. J. and Uchida, S., 2006, "The Effect Of Coolant Injection On The Endwall Flow Of A High Pressure Turbine", Proceedings of ASME Turbo Expo 2006, GT2006-91060

[9] Schuepbach, P., Abhari, R. S., Rose, M., Germain, T., Raab, I., Gier, J., 2010, "Effects of Suction and Injection Purge-Flow on the Secondary Flow Structures of a High-Work Turbine", Journal of Turbomachinery, Vol. 132

[10] Regina, K., Kalfas, A. I. and Abhari, R. S., 2012, "Experimental Investigation of Purge Flow Effects on a High Pressure Turbine Stage", Proceedings of ASME Turbo Expo 2012, GT2012-69466

[11] Behr, T., Kalfas, A. I. and Abhari, R.S., 2007, "Unsteady Flow Physics and Performance of a One-and-1/2-Stage Unshrouded High Work Turbine", Journal of Turbomachinery, Vol. 129, pp. 348-359

[12] Kupferschmied, P., Köppel, P., Gizzi, W., Roduner, C. and Gyarmathy, G., 2000, "Time-resolved flow measurements with fast-response aerodynamic probes in turbomachines", Meas. Sci. Technol. 11, pp. 1036-1054

[13] Pfau, A., Schlienger, J., Kalfas, A. I. and Abhari, R. S., 2003, "Unsteady 3-dimensional flow measurement using a miniature virtual 4 sensor fast response aerodynamic probe (FRAP)", Proceedings of ASME Turbo Expo 2003, GT2003-39128

[14] Cao, C., Chew, J. W., Millington, P. R. and Hogg, S. I., 2003, "Interaction Of Rim Seal And Annulus Flows In An Axial Flow Turbine", Proceedings of ASME Turbo Expo 2003, GT2003-38368

[15] Schuepbach, P., 2009, "Influence of Rim Seal Purge Flow on the Performance of an End Wall Profiled Axial Turbine", PhD thesis, ETH Zurich